Iterative Pole–Zero model updating

Iterative Pole-Zero Model Updating: A Combined Sensitivity Approach

M. Dorosti[a,b,*], R.H.B. Fey[a], M.F. Heertjes[a,b], H. Nijmeijer[a]

[a]*Mechanical Engineering Department, Eindhoven University of Technology, 5600 MB Eindhoven, the Netherlands*
[b]*ASML, De Run 6501, 5504 DR Veldhoven, the Netherlands*

Abstract

A crucial step in the control of a weakly damped high precision motion system is having an accurate dynamic model of the system from actuators to sensors and to the unmeasured performance variables. A (reduced) Finite Element (FE) model may be a good candidate apart from the fact that it often does not sufficiently match with the real system especially when it comes to machine-to-machine variation. To improve the dynamic properties of the FE model toward the dynamic properties of a specific machine, an Iterative Pole-Zero (IPZ) model updating procedure is used that updates numerical poles and zeros of Frequency Response Functions (FRFs) towards measured poles and zeros, which can be extracted from the measured FRFs. It is assumed that in a practical situation, the model (physical) parameters that cause discrepancy with the real structure are unknown. Therefore, the updating parameters will be the eigenvalues of the stiffness and/or damping (sub)matrix. In this paper, an IPZ model updating is introduced which combines the sensitivity functions of both poles and zeros (with respect to the corresponding updating parameters) together with the cross sensitivity functions between poles and zeros. The procedure is verified first using simulated experiments of a pinned-sliding beam structure and then using non-collocated FRF measurement results from a cantilever beam setup.

Keywords: FE model, Model updating, Pole, Zero, Combined Sensitivity, Generic parameters, Unmeasured performance variable, weakly damped systems

1. Introduction

High-precision motion stages are an important part of high-tech systems such as wafer scanners and microscopes [1–3]. Motion stages are basically made of lightly damped flexible structures resulting in flexible dynamic behavior of the system. For accurate positioning of stages, knowledge of an accurate yet low-order parametric model of the system from actuators to the sensors and to the unmeasured performance variables at the Point-Of-Interest (POI) is unavoidable. In many situations, identification techniques are used for calculation of the parametric model from actuators

*Corresponding author
Email addresses: M.Dorosti@tue.nl (M. Dorosti), R.H.B.Fey@tue.nl (R.H.B. Fey), M.F.Heertjes@tue.nl (M.F. Heertjes), H.Nijmeijer@tue.nl (H. Nijmeijer)

to the sensors. However, in other situations where the performance variable is located in a different location than the sensor location, identification techniques cannot be used. In these situations, reduced-order FE models may be used to accurately predict the performance variables. However, FE models normally do not sufficiently match with the real structure due to simplification in FE modeling or due to manufacturing tolerances.

To improve the accuracy of a FE model in terms of matching the dynamic behavior with the real structure, model updating techniques are well-known tools. In principle there are two types of model updating techniques: direct methods and iterative methods. In [4], it is shown that iterative methods generally give better matching of FRFs with experimental data and that predictions based on iterative methods are better than those based on direct methods beyond the considered frequency range. Within the iterative methods, there are two categories of model updating techniques. The first category contains modal-based techniques and is concerned with updating modal properties such as eigenfrequencies, antiresonance frequencies, and mode shapes in an attempt to reduce the residuals between numerical and measured modal quantities, e.g. see [5–7]. The second category contains FRF-based techniques and attempts at reducing the residuals between numerical and measured FRFs directly, see e.g. [8–10]. In [11], a comparative study is given on the model updating approaches using either modal or FRF residuals.

One of the key issues in model updating is how to select appropriate design parameters. In some situations, it is clear which (physical) model parameter values are uncertain. In other situations, e.g. for geometrically complex structures with many mechanical connections, it may be far from trivial to identify which physical parameters are causing differences between the numerical and the experimental target quantities. Even if the uncertain physical parameter is known, derivation of the sensitivity of the model to that parameter may be computationally highly demanding. Moreover, the relation between the model and the physical parameters is often lost as soon as model reduction is applied. In those situations, generic parameters may be better candidates for model updating. Generic element parameterization is for example based on allowing changes to the eigenvalues and eigenvectors of the stiffness matrices of the structural elements or substructures [12]. Performance of FE model updating techniques under selection of different classes of parameters is compared in [13]. It is important to mention that having an (over)determined model updating problem is often desirable, i.e. having fewer or the same number of design parameters compared to the number of measured quantities [5]. This is because having more design parameters than residuals increases the chance of creating an ill-conditioned problem and may also lead to physically unacceptable parameter updates.

Most of the modal-based model updating techniques are concerned with updating the eigenfrequencies, see e.g. [5, 6]. Recently, some effort has been dedicated to include the effect of antiresonances in the model updating, see [14–18]. However, all of these model updating techniques are based on updating physical design parameters. Contrary, in IPZ model updating, the eigenvalues of the stiffness and/or damping matrix of the (sub)structure are introduced as the generic parameters. This is done because errors in stiffness and/or damping modeling are more likely to occur than errors in mass modeling. The choice for these generic parameters comes with the advantages that the number of design parameters will be limited, and that the exact location of the model error does not need to be known.

IPZ model updating in general tries to reduce the pole and zero residuals between numerical

and measured values, which are obtained from a few FRF measurements from the existing actuator/sensor configuration. In this paper, an IPZ model updating technique is introduced which uses a standard gradient-based technique to update generic parameters such that the poles and zeros of a reduced numerical model iteratively converge to their experimentally estimated counterparts. To do so, equations are derived to calculate increments for the pole and zero generic parameters simultaneously. This is done by using combined sensitivities. Not only the pole sensitivities w.r.t. the pole generic parameters and the zero sensitivities w.r.t. the zero generic parameters are used, but also the cross sensitivities between the poles and the zero generic parameters (and vice versa) are incorporated. Subsequently, first the stiffness (or damping) structure matrix and subsequently the substructure (or damping) stiffness matrices are updated sequentially.

In a nutshell, contributions of IPZ model updating can be summarized in the following areas. First, updating of complex-valued poles and zeros is done instead of (mostly used in the literature) real-valued resonance and antiresonance frequencies. In other words, the damping matrix is updated as well as the stiffness matrix. The majority of the existing updating procedures are dedicated to undamped structures. Second, model updating is carried out using generic parameters instead of physical parameters which is suited for geometrically complex structures where the erroneous physical parameters are hardly known. Third, model updating is performed on the reduced-order model.

The remainder of the paper is organized as follows. Section 2 is dedicated to a short recap on model reduction including residual flexibility, which will be used in IPZ model updating. In Section 3, the theoretical framework of IPZ model updating using combined sensitivities is discussed. Simulation is a powerful tool for verification of techniques, since we have access to the expected results. Therefore, in Section 4, a pinned-sliding beam structure is introduced as a case study to verify the IPZ model updating technique with combined sensitivities. The IPZ model updating technique with combined sensitivities is experimentally validated through non-collocated FRF measurement results from a cantilever beam setup in Section 5. Finally, some conclusions are drawn in Section 6.

2. Model Reduction

Updating a FE model of a complex system with many Degrees-Of-Freedom (DOFs), typically in the order of 10^6, is generally computationally expensive. Moreover, from a system and control point of view we are often interested in a specific frequency range which may include rigid body modes as well as a limited number of flexible modes that have relevant contributions to the input-output behavior of the system. Therefore, the original FE model will be reduced. It is assumed that the linear dynamic behavior of a mechanical structure can be described by

$$\mathbf{M}_n\ddot{\mathbf{q}}_n + \mathbf{B}_n\dot{\mathbf{q}}_n + \mathbf{K}_n\mathbf{q}_n = \mathbf{f}_n, \tag{1}$$

with $\mathbf{q}_n \in \mathbb{R}^{n\times 1}$ the vector with n DOFs, $\mathbf{f}_n \in \mathbb{R}^{n\times 1}$ the external load vector, $\mathbf{M}_n = \mathbf{M}_n^T \succ 0$ the positive-definite mass matrix, $\mathbf{B}_n = \mathbf{B}_n^T \succeq 0$ the positive semi-definite damping matrix, $\mathbf{K}_n = \mathbf{K}_n^T \succeq 0$ the positive semi-definite stiffness matrix, and $\mathbf{M}_n, \mathbf{B}_n, \mathbf{K}_n \in \mathbb{R}^{n\times n}$. Using a model

reduction technique based on eigenmodes and residual flexibility modes, the following reduced-order dynamic equation is derived

$$\mathbf{M}_r\ddot{\mathbf{q}}_r + \mathbf{B}_r\dot{\mathbf{q}}_r + \mathbf{K}_r\mathbf{q}_r = \mathbf{f}_r, \tag{2}$$

with the reduced order mass matrix $\mathbf{M}_r = \mathbf{M}_r^T = {\mathbf{\Phi}_s^{-1}}^T\mathbf{\Phi}_r^T\mathbf{M}_n\mathbf{\Phi}_r\mathbf{\Phi}_s^{-1} \succ 0$, damping matrix $\mathbf{B}_r = \mathbf{B}_r^T = {\mathbf{\Phi}_s^{-1}}^T\mathbf{\Phi}_r^T\mathbf{B}_n\mathbf{\Phi}_r\mathbf{\Phi}_s^{-1} \succeq 0$, and stiffness matrix $\mathbf{K}_r = \mathbf{K}_r^T = {\mathbf{\Phi}_s^{-1}}^T\mathbf{\Phi}_r^T\mathbf{K}_n\mathbf{\Phi}_r\mathbf{\Phi}_s^{-1} \succeq 0$, $\mathbf{M}_r, \mathbf{B}_r, \mathbf{K}_r \in \mathbb{R}^{r\times r}$, and $\mathbf{f}_r = {\mathbf{\Phi}_s^{-1}}^T\mathbf{\Phi}_r^T\mathbf{f}_n \in \mathbb{R}^{r\times 1}$ the reduced external load column. $\mathbf{\Phi}_r \in \mathbb{R}^{n\times r}$ is a subset of the mode shape matrix, which column-wise consists of (a) rigid-body modes (if present), (b) a selected number of low-frequency modes, and (c) residual flexibility modes defined for externally loaded DOFs. Row-wise $\mathbf{\Phi}_r$ consists of all DOFs. The square matrix $\mathbf{\Phi}_s \in \mathbb{R}^{r\times r}$ is a subset of $\mathbf{\Phi}_r$, which column-wise consists of the same modes as in $\mathbf{\Phi}_r$, but row-wise consists of only desired physical DOFs including actuator, sensor, and unmeasured performance variable DOFs. This has been explained in more detail in [7].

3. Iterative Pole-Zero Model Updating Using Combined Sensitivities

Imagine that in a motion system, an accurate prediction of a performance variable (for a location different than the sensor location) is needed. Assume that an FRF measurement from an actuator to a sensor is available. Also assume that the FE model of the system is available but the generated numerical FRF between the actuator and the sensor shows discrepancy with the measured FRF. A solution to this problem is to first reduce the FE model of the system, and then update the reduced model using poles and zeros derived from the measured FRF. Subsequently, the updated reduced FE model can be used for accurate prediction of the performance variable z.

Using the reduced-order dynamic equation in (2), the FRF corresponding to a sensor at DOF i and an actuator at DOF j can be described as

$$\mathbf{G}_{ij}(\omega) = \frac{\det(-\omega^2\mathbf{M}_s + j\omega\mathbf{B}_s + \mathbf{K}_s)}{\det(-\omega^2\mathbf{M}_r + j\omega\mathbf{B}_r + \mathbf{K}_r)}, \tag{3}$$

where $\mathbf{M}_s, \mathbf{B}_s, \mathbf{K}_s$ are the so-called substructure matrices which are constructed from the reduced-order matrices $\mathbf{M}_r, \mathbf{B}_r, \mathbf{K}_r$ respectively, by eliminating the i^{th} column and the j^{th} row corresponding to the sensor and actuator DOFs [18]. Note that if $i \neq j$, the substructure matrices will generally be non-symmetric. Now assume that m_p experimental poles ($\boldsymbol{\lambda}_{p,e} \in \mathbb{C}^{m_p\times 1}$) and m_z experimental zeros ($\boldsymbol{\lambda}_{z,e} \in \mathbb{C}^{m_z\times 1}$) are extracted from the measured FRF using modal parameter fit techniques [19, 20]. The numerical poles ($\boldsymbol{\lambda}_{p,n}$) and zeros ($\boldsymbol{\lambda}_{z,n}$) of the reduced-order model in (3) are calculated by solving the eigenvalue problem

$$(\lambda_{p,n}^2\mathbf{M}_r + \lambda_{p,n}\mathbf{B}_r + \mathbf{K}_r)\boldsymbol{\psi}_p = 0, \tag{4}$$

and

$$(\lambda_{z,n}^2\mathbf{M}_s + \lambda_{z,n}\mathbf{B}_s + \mathbf{K}_s)\boldsymbol{\psi}_z = 0, \tag{5}$$

respectively. Note that subscripts p, z, e, and n stand for pole, zero, experimental, and numerical, respectively. The numerical poles/zeros will in general differ from the measured values, hence the former need to be updated.

In order to update the reduced-order model, the following combined quadratic pole-zero error functional

$$\epsilon_i(\boldsymbol{\theta}) = \left(\begin{bmatrix} \boldsymbol{\lambda}_{p,e} \\ \boldsymbol{\lambda}_{z,e} \end{bmatrix} - \begin{bmatrix} \boldsymbol{\lambda}_{p,n}(\boldsymbol{\theta}) \\ \boldsymbol{\lambda}_{z,n}(\boldsymbol{\theta}) \end{bmatrix}_i \right)^H \mathbf{W}_{\lambda_i} \left(\begin{bmatrix} \boldsymbol{\lambda}_{p,e} \\ \boldsymbol{\lambda}_{z,e} \end{bmatrix} - \begin{bmatrix} \boldsymbol{\lambda}_{p,n}(\boldsymbol{\theta}) \\ \boldsymbol{\lambda}_{z,n}(\boldsymbol{\theta}) \end{bmatrix}_i \right), \tag{6}$$

can be iteratively (i refers to iteration step) minimized using the updating parameters $\boldsymbol{\theta}$. The diagonal weighting matrix $\mathbf{W}_{\lambda_i} \succ 0$ is applied in order to have an equal contribution of the relative errors from each pole and zero, which equals

$$\mathbf{W}_{\lambda_i} = \lambda^2_{\text{max,i}} \begin{bmatrix} |\lambda_{p,n,1}|^{-2} & 0 & 0 \\ 0 & \ddots & 0 \\ 0 & 0 & |\lambda_{z,n,m_z}|^{-2} \end{bmatrix}_i, \tag{7}$$

where $\lambda_{\text{max,i}}$ is the maximum modulus among modulus of the entries of $\boldsymbol{\lambda}_{p,n}$ and $\boldsymbol{\lambda}_{z,n}$ in iteration i. Note that $\mathbf{W}_{\lambda_i}$ is updated in each iteration based on the new values of the numerical poles and zeros.

A subsequent step is to choose the updating parameters $\boldsymbol{\theta}$. In geometrically complex structures with many mechanical connections, it is not easy to identify which physical parameters are causing differences between the numerical and experimental poles/zeros. Even if the uncertain physical parameter is known, the relation between the model and the physical parameter is lost as soon as model reduction is applied. In these situations, generic parameters can be used. In the case of weak damping, it can be assumed that the error in the model is dominantly present in the stiffness matrix rather than in the mass matrix. Assuming that no information is available on possible locations of stiffness errors in the model, it is proposed to use only a limited number of eigenvalues of the reduced-order stiffness (sub)structure matrix as generic parameters to be updated. The eigenvalue decomposition of the reduced-order stiffness matrix $\mathbf{K}_r$ is given by

$$\mathbf{K}_r = \mathbf{V}_p \boldsymbol{\Sigma}_p \mathbf{V}_p^T, \tag{8}$$

where $\mathbf{V}_p \in \mathbb{R}^{r \times r}$ is a square matrix containing column-wise the real static stiffness mode shapes and where $\boldsymbol{\Sigma}_p \in \mathbb{R}^{r \times r}$ is a diagonal matrix containing the corresponding real eigenvalues of the reduced-order stiffness matrix, i.e., $\boldsymbol{\Sigma}_p = \text{diag}(\sigma_{p,1}, \cdots, \sigma_{p,r})$. The generic parameters $\boldsymbol{\theta}_p$ needed to update a selected number of the low-frequency poles are in general a selected number of the smallest eigenvalues of $\mathbf{K}_r$, i.e. $\boldsymbol{\theta}_p \subset \{\sigma_{p,1}, \cdots, \sigma_{p,r}\}$, where $\boldsymbol{\theta}_p \in \mathbb{R}^{q_p \times 1}$ and $q_p \leq r$. Note that if the structure has rigid body modes, the zero eigenvalues corresponding to these rigid body modes have to be excluded from the set of generic parameters.

Likewise, the generic parameters $\boldsymbol{\theta}_z$ needed to update a selected number of the low-frequency zeros are a selected number of the smallest eigenvalues of the reduced-order substructure stiffness matrix $\mathbf{K}_s$, which are derived from

$$\mathbf{K}_s = \mathbf{V}_z \boldsymbol{\Sigma}_z \mathbf{V}_z^T, \tag{9}$$

where $\boldsymbol{\Sigma}_z \in \mathbb{R}^{r-1 \times r-1}$ is a diagonal matrix containing the corresponding real eigenvalues of $\mathbf{K}_s$, i.e., $\boldsymbol{\Sigma}_z = \text{diag}(\sigma_{z,1}, \cdots, \sigma_{z,r-1})$. Thus, $\boldsymbol{\theta}_z \subset \{\sigma_{z,1}, \cdots, \sigma_{z,r-1}\}$, where $\boldsymbol{\theta}_z \in \mathbb{R}^{q_z \times 1}$ and $q_z \leq r-1$. Summarizing, the generic parameters $\boldsymbol{\theta}^T = [\boldsymbol{\theta}_p^T \boldsymbol{\theta}_z^T]$ will be updated to bring the numerical eigenvalues $\boldsymbol{\lambda}_{p,n}$ and $\boldsymbol{\lambda}_{z,n}$ close to their experimental counterparts.

In order to find an analytical solution to minimize (6) , the entries $\boldsymbol{\lambda}_{p,n}(\boldsymbol{\theta})$ and $\boldsymbol{\lambda}_{z,n}(\boldsymbol{\theta})$ can be replaced by their first-order Taylor series approximations around $\boldsymbol{\theta}_i$, i.e.

$$\lambda_{n,i+1}(\boldsymbol{\theta}_{i+1}) \approx \lambda_{n,i}(\boldsymbol{\theta}_i) + \frac{\partial \lambda_{n,i}(\boldsymbol{\theta}_i)}{\partial \boldsymbol{\theta}} \Delta\boldsymbol{\theta}_i. \tag{10}$$

Therefore, ϵ_i in (6) can be approximated by

$$\epsilon_i^*(\boldsymbol{\theta}) = \Delta\mathbf{r}_i^H(\boldsymbol{\theta}) \mathbf{W}_{\lambda_i} \Delta\mathbf{r}_i(\boldsymbol{\theta}), \tag{11}$$

where

$$\Delta\mathbf{r}_i(\boldsymbol{\theta}) = \Delta\boldsymbol{\lambda}_i(\boldsymbol{\theta}) - \mathbf{S}_i(\boldsymbol{\theta})\Delta\boldsymbol{\theta}, \tag{12}$$

where

$$\Delta\boldsymbol{\lambda}_i(\boldsymbol{\theta}) = \begin{bmatrix} \boldsymbol{\lambda}_{p,e} \\ \boldsymbol{\lambda}_{z,e} \end{bmatrix} - \begin{bmatrix} \boldsymbol{\lambda}_{p,n}(\boldsymbol{\theta}) \\ \boldsymbol{\lambda}_{z,n}(\boldsymbol{\theta}) \end{bmatrix}_i, \tag{13}$$

and

$$\mathbf{S}_i(\boldsymbol{\theta}) = \begin{bmatrix} \mathbf{S}_{pp} & \mathbf{S}_{pz} \\ \mathbf{S}_{zp} & \mathbf{S}_{zz} \end{bmatrix}_i. \tag{14}$$

$\mathbf{S}_i(\boldsymbol{\theta})$ in (14) represents the sensitivity matrix which includes the sensitivity of the poles w.r.t. the pole design parameters ($\mathbf{S}_{pp} = \partial\boldsymbol{\lambda}_{p,n}(\boldsymbol{\theta}_p)/\partial\boldsymbol{\theta}_p$), the sensitivity of the zeros w.r.t. the zero design parameters ($\mathbf{S}_{zz} = \partial\boldsymbol{\lambda}_{z,n}(\boldsymbol{\theta}_z)/\partial\boldsymbol{\theta}_z$), and the cross sensitivity of the poles w.r.t. the zero design parameters ($\mathbf{S}_{pz} = \partial\boldsymbol{\lambda}_{p,n}(\boldsymbol{\theta}_z)/\partial\boldsymbol{\theta}_z$) and vice versa ($\mathbf{S}_{zp} = \partial\boldsymbol{\lambda}_{z,n}(\boldsymbol{\theta}_p)/\partial\boldsymbol{\theta}_p$). It is important to mention that (11) is a good approximation of (6) in the vicinity of $\lambda_{n,i}(\boldsymbol{\theta})$. Note that due to the assumption of weak damping, in general the imaginary part of $\Delta\boldsymbol{\lambda}_i$ and hence the imaginary part of $\Delta\mathbf{r}_i$ will be dominant over the real part.

Due to numerical issues, minimizing (11) may lead to an ill-conditioned problem. Using regularization techniques [21–23], this problem can be overcome. In that sense, (11) is replaced with the following quadratic error functional

$$\epsilon_i^*(\boldsymbol{\theta}) = \Delta\mathbf{r}_i^H(\boldsymbol{\theta}) \mathbf{W}_{\lambda_i} \Delta\mathbf{r}_i(\boldsymbol{\theta}) + \alpha^2 \Delta\boldsymbol{\theta}_i^T \mathbf{W}_{\theta_i} \Delta\boldsymbol{\theta}_i, \tag{15}$$

where the regularization parameter α is used to balance between the measurement residuals and the parameter changes, and

$$\mathbf{W}_{\theta_i} = \frac{\text{mean}(\text{diag}(\boldsymbol{\Gamma}))}{\text{mean}(\text{diag}(\boldsymbol{\Gamma}^{-1}))} \boldsymbol{\Gamma}^{-1} \succ 0, \tag{16}$$

as suggested by [24] in an attempt to have an equal contribution of the elements $\Delta\boldsymbol{\theta}_i$, with

$$\boldsymbol{\Gamma} = \text{diag}(\mathbf{S}_i^H \mathbf{W}_{\lambda_i} \mathbf{S}_i)). \tag{17}$$

In our case, we will always choose $q^p + q^z \leqslant m^p + m^z$ to make the optimization problem (over)determined. Hence, a least squares approach is used. Minimizing (15) with regard to $\Delta\boldsymbol{\theta}_i$ requiring that $\partial\epsilon_i/\partial\Delta\boldsymbol{\theta}_i = 0$ leads to the following equation:

$$\text{Re}\left(\mathbf{S}_i^H \mathbf{W}_{\lambda_i} \mathbf{S}_i + \alpha^2 \mathbf{W}_{\theta_i}\right) \Delta\boldsymbol{\theta}_i = \text{Re}\left(\mathbf{S}_i^H \mathbf{W}_{\lambda_i} \Delta\boldsymbol{\lambda}_i\right), \tag{18}$$

which can be solved for $\Delta\boldsymbol{\theta}_i$ to update the parameters. The updated parameters $\boldsymbol{\theta}$ in the $i+1$ iteration become

$$\boldsymbol{\theta}_{i+1} = \boldsymbol{\theta}_i + \beta\Delta\boldsymbol{\theta}_i, \tag{19}$$

where $\beta > 0$ is a scaling factor which is equal to one in a classical Newton-Raphson scheme. The damped Newton method [25], where $0 < \beta < 1$, may improve convergence toward a (local) minimum of (15); in some cases, using $1 < \beta < 2$, speeds up the convergence rate. In case ϵ_i is decreasing toward a (local) minimum, the iteration process is stopped using the following stop criterion

$$|\epsilon_i - \epsilon_{i-1}| \leq \delta, \tag{20}$$

where δ is a sufficiently small number. This basically means that when the error (ϵ_i) is not decreasing much further, the algorithm will stop; note that an appropriate value of δ also depends on $\mathbf{W}_{\lambda_i}$ and $\mathbf{W}_{\theta_i}$.

Entries of the sensitivity matrix $\mathbf{S}_i$ in (14) can be derived as follows. The sensitivity of a pole ($\lambda_{p,n}$) w.r.t. an eigenvalue of the reduced-order stiffness matrix (θ_p) can be derived from (4), which is given by

$$\frac{\partial\lambda_{p,n}(\theta_p)}{\partial\theta_p} = \frac{{\boldsymbol{\psi}_p}^T \frac{\partial\mathbf{K}_r}{\partial\theta_p}\boldsymbol{\psi}_p}{2\lambda_{p,n}{\boldsymbol{\psi}_p}^T\mathbf{M}_r\boldsymbol{\psi}_p + {\boldsymbol{\psi}_p}^T\mathbf{B}_r\boldsymbol{\psi}_p}, \tag{21}$$

where $\boldsymbol{\psi}_p$ is the eigenvector corresponding to the pole $\lambda_{p,n}$, and where

$$\frac{\partial\mathbf{K}_r}{\partial\theta_p} = \mathbf{v}_p\mathbf{v}_p^{inv^T}, \tag{22}$$

with $\mathbf{v}_p$ denoting a column of $\mathbf{V}_p$ corresponding to θ_p and $\mathbf{v}_p^{inv^T}$ the corresponding row in $\mathbf{V}_p^{-1}$ or $\mathbf{V}_p^T$. From the numerator of (21) it is clear that the sensitivity is relatively large when the angle between $\boldsymbol{\psi}_p$ and $\mathbf{v}_p$ is small. Contrarily, a relatively small sensitivity is obtained when $\boldsymbol{\psi}_p$ and $\mathbf{v}_p$ are (nearly) orthogonal. The sensitivity of a zero ($\lambda_{z,n}$) w.r.t. an eigenvalue of the substructure reduced-order stiffness matrix (θ_z) is derived from (5), which is calculated by

$$\frac{\partial\lambda_{z,n}(\theta_z)}{\partial\theta_z} = \frac{{\boldsymbol{\psi}_z}^T \frac{\partial\mathbf{K}_s}{\partial\theta_z}\boldsymbol{\psi}_z}{2\lambda_{z,n}{\boldsymbol{\psi}_z}^T\mathbf{M}_s\boldsymbol{\psi}_z + {\boldsymbol{\psi}_z}^T\mathbf{B}_s\boldsymbol{\psi}_z}, \tag{23}$$

where $\boldsymbol{\psi}_z$ is the eigenvector corresponding to the zero $\lambda_{z,n}$, and where

$$\frac{\partial\mathbf{K}_s}{\partial\theta_z} = \mathbf{v}_z\mathbf{v}_z^{inv^T}, \tag{24}$$

with $\mathbf{v}_z$ denoting a column of $\mathbf{V}_z$ corresponding to θ_z and $\mathbf{v}_z^{inv^T}$ the corresponding row in $\mathbf{V}_z^{-1}$ or $\mathbf{V}_z^T$. The cross sensitivities, i.e. the sensitivity of a pole w.r.t. θ_z and the sensitivity of a zero w.r.t. θ_p are respectively given by

$$\frac{\partial\lambda_{p,n}(\theta_z)}{\partial\theta_z} = \frac{{\boldsymbol{\psi}_p}^T \frac{\partial\mathbf{K}_r}{\partial\theta_z}\boldsymbol{\psi}_p}{2\lambda_{p,n}{\boldsymbol{\psi}_p}^T\mathbf{M}_r\boldsymbol{\psi}_p + {\boldsymbol{\psi}_p}^T\mathbf{B}_r\boldsymbol{\psi}_p}, \tag{25}$$

and

$$\frac{\partial \lambda_{z,n}(\theta_p)}{\partial \theta_p} = \frac{{\boldsymbol{\psi}_z}^T \frac{\partial \mathbf{K}_s}{\partial \theta_p} \boldsymbol{\psi}_z}{2\lambda_{z,n} {\boldsymbol{\psi}_z}^T \mathbf{M}_s \boldsymbol{\psi}_z + {\boldsymbol{\psi}_z}^T \mathbf{B}_s \boldsymbol{\psi}_z}. \tag{26}$$

Regarding the derivation of $\partial \mathbf{K}_r / \partial \theta_z$ and $\partial \mathbf{K}_s / \partial \theta_p$, it has been mentioned that the reduced-order substructure stiffness matrix ($\mathbf{K}_s$) is derived from the reduced-order stiffness matrix ($\mathbf{K}_r$) by deleting the appropriate row/column corresponding to the actuator/sensor DOF. Therefore, $\mathbf{K}_r$ can be written as

$$\mathbf{K}_r = \mathbf{K}_{r,s} + \Delta \mathbf{K}_r, \tag{27}$$

where $\mathbf{K}_{r,s}$ is partitioned such that

$$\mathbf{K}_{r,s} = \left[\begin{array}{c|c|c} \mathbf{K}_{s,1} & 0 & \mathbf{K}_{s,2} \\ \hline 0 & 0 & 0 \\ \hline \mathbf{K}_{s,3} & 0 & \mathbf{K}_{s,4} \end{array}\right], \tag{28}$$

and

$$\Delta \mathbf{K}_r = \left[\begin{array}{c|c|c} 0 & \Delta \mathbf{k}_{r,1} & 0 \\ \hline \Delta \mathbf{k}_{r,2}^T & \Delta k_{r,3} & \Delta \mathbf{k}_{r,4}^T \\ \hline 0 & \Delta \mathbf{k}_{r,5} & 0 \end{array}\right], \tag{29}$$

the latter representing the deleted part of the stiffness matrix. $\mathbf{K}_s$ is derived from (28), i.e

$$\mathbf{K}_s = \left[\begin{array}{c|c} \mathbf{K}_{s,1} & \mathbf{K}_{s,2} \\ \hline \mathbf{K}_{s,3} & \mathbf{K}_{s,4} \end{array}\right]. \tag{30}$$

Combining (30) and (24) gives

$$\frac{\partial \mathbf{K}_s}{\partial \theta_z} = \mathbf{v}_z \mathbf{v}_z^{inv^T} = \left[\begin{array}{c|c} \frac{\partial \mathbf{K}_{s,1}}{\partial \theta_z} & \frac{\partial \mathbf{K}_{s,2}}{\partial \theta_z} \\ \hline \frac{\partial \mathbf{K}_{s,3}}{\partial \theta_z} & \frac{\partial \mathbf{K}_{s,4}}{\partial \theta_z} \end{array}\right]. \tag{31}$$

Now taking the derivative of $\mathbf{K}_r$, see (27), with regard to θ_z and using (28) results in

$$\frac{\partial \mathbf{K}_r}{\partial \theta_z} = \frac{\partial \mathbf{K}_{r,s}}{\partial \theta_z} = \left[\begin{array}{c|c|c} \frac{\partial \mathbf{K}_{s,1}}{\partial \theta_z} & 0 & \frac{\partial \mathbf{K}_{s,2}}{\partial \theta_z} \\ \hline 0 & 0 & 0 \\ \hline \frac{\partial \mathbf{K}_{s,3}}{\partial \theta_z} & 0 & \frac{\partial \mathbf{K}_{s,4}}{\partial \theta_z} \end{array}\right]. \tag{32}$$

Partitioning (22) according to (27)-(29) leads to

$$\frac{\partial \mathbf{K}_r}{\partial \theta_p} = \mathbf{v}_p \mathbf{v}_p^{inv^T} = \left[\begin{array}{c|c|c} \frac{\partial \mathbf{K}_{r,1}}{\partial \theta_p} & \frac{\partial \mathbf{k}_{r,2}}{\partial \theta_p} & \frac{\partial \mathbf{K}_{r,3}}{\partial \theta_p} \\ \hline \frac{\partial \mathbf{k}_{r,4}}{\partial \theta_p}^T & \frac{\partial k_{r,5}}{\partial \theta_p} & \frac{\partial \mathbf{k}_{r,6}}{\partial \theta_p}^T \\ \hline \frac{\partial \mathbf{K}_{r,7}}{\partial \theta_p} & \frac{\partial \mathbf{k}_{r,8}}{\partial \theta_p} & \frac{\partial \mathbf{K}_{r,9}}{\partial \theta_p} \end{array}\right], \tag{33}$$

which through (30) implies that

$$\frac{\partial \mathbf{K}_s}{\partial \theta_p} = \left[\begin{array}{c|c} \frac{\partial \mathbf{K}_{r,1}}{\partial \theta_p} & \frac{\partial \mathbf{K}_{r,3}}{\partial \theta_p} \\ \hline \frac{\partial \mathbf{K}_{r,7}}{\partial \theta_p} & \frac{\partial \mathbf{K}_{r,9}}{\partial \theta_p} \end{array}\right]. \tag{34}$$

3.1. IPZ model updating algorithm

In summary, the proposed IPZ model updating algorithm reads as follows:

1. Preparation phase
   (a) For the measured FRF, choose the frequency range of interest in which the model needs to be updated; identify the experimental values of the poles and zeros in this frequency range.
   (b) From the FE model select the desired physical DOFs including the actuators, sensors, and unmeasured performance variables at the POI.
   (c) Apply model reduction as discussed in Section 2.
   (d) Select an appropriate value for δ in the stop criterion (20).
   (e) Select the regularization parameter α in (15) and the convergence rate parameter β in (19); here α is chosen at 0.1, and the initial value for β is generally chosen as $\beta = 1$; one may increase or decrease α depending on the condition number and β to control the convergence rate.
2. IPZ model updating
   (a) Select a number of the (smallest) eigenvalues σ_p of the reduced stiffness matrix $\mathbf{K}_r$, sensitive to the selected poles, as the generic parameters $\boldsymbol{\theta}_p$.
   (b) Select a number of the (smallest) eigenvalues σ_z of the substructure reduced stiffness matrix $\mathbf{K}_s$, sensitive to the selected zeros, as the generic parameters $\boldsymbol{\theta}_z$.
   (c) Calculate the values of poles and zeros using (4) and (5).
   (d) Match the experimental poles and zeros with their numerical counterparts from the FE model.
   (e) Calculate the sensitivity matrix $\mathbf{S}_i$ based on (21), (23), (25), and (26).
   (f) Define $\mathbf{W}_{\lambda_i}$, see (7), and $\mathbf{W}_{\theta_i}$, see (16).
   (g) Calculate the condition number of $\mathbf{S}_i^H \mathbf{W}_{\lambda_i} \mathbf{S}_i$; in the case that the condition number is below 10^5 use $\alpha = 0$; otherwise, use the initially selected α.
   (h) Calculate $\Delta\boldsymbol{\lambda}_i$ in (12).
   (i) Calculate $\Delta\boldsymbol{\theta}_i$ and $\boldsymbol{\theta}_{i+1}$ according to (18) and (19).
   (j) Incorporate the updated generic parameters $\boldsymbol{\theta}_p$ into (8) to calculate the updated structure stiffness matrix $\mathbf{K}_r^u$.
   (k) Incorporate the updated generic parameters $\boldsymbol{\theta}_z$ into (9) to calculate the updated substructure stiffness matrix $\mathbf{K}_s^u$.
   (l) Use (27) - (28) to include $\mathbf{K}_s^u$ into $\mathbf{K}_r^u$ and construct the updated stiffness matrix $\mathbf{K}^u$.
3. Finalizing phase
   (a) Calculate ϵ_i in (6) based on $\mathbf{K}^u$.

(b) Check whether the stop criterion in (20) is satisfied; if not, return to step 2 (c) using the updated stiffness matrix $\mathbf{K}^u$; the iteration process stops when the stop criterion in (20) is satisfied.

Note that in order to update the damping, the damping matrix will be used instead of the stiffness matrix which basically applies for the same procedure. Typically, since weak damping is assumed, updating of the damping matrix will be carried out after updating of the stiffness matrix, because weak damping will mainly influence the real part of the poles and zeros and hardly influences the imaginary parts. Also note that, since the substructure matrix is non-symmetric for any non-collocated actuator/sensor configuration, the updated stiffness/damping matrix (though physically undesirable) may become slightly non-symmetric. Furthermore, it is important to note that using the eigenvalues of the (sub)structure matrix as generic updating parameters may contribute to $\mathbf{S}_i$ being of full rank, hence to better conditioning of the problem.

3.2. Convergence

Since the IPZ model updating approach is gradient-based, minimization of (15) will often results in a (local) minimum. This can be shown as follows. Taking the derivative of ϵ_i^* in (15) with respect to $\Delta\boldsymbol{\theta}_i$ yields

$$\frac{\partial \epsilon_i^*}{\partial \Delta\boldsymbol{\theta}_i} = -2\Delta\mathbf{r}_i^H \mathbf{W}_{\lambda_i} \mathbf{S}_i + 2\alpha^2 \Delta\boldsymbol{\theta}_i{}^T \mathbf{W}_{\theta_i}, \tag{35}$$

which using (12) can be rewritten as

$$\frac{\partial \epsilon_i^*}{\partial \Delta\boldsymbol{\theta}_i} = -2\Delta\boldsymbol{\lambda}_i^H \mathbf{W}_{\lambda_i} \mathbf{S}_i + 2\Delta\boldsymbol{\theta}_i{}^T \left(\mathbf{S}_i^H \mathbf{W}_{\lambda_i} \mathbf{S}_i + \alpha^2 \mathbf{W}_{\theta_i} \right), \tag{36}$$

and which is affine in $\Delta\boldsymbol{\theta}_i$. Taking the second derivative of ϵ_i with respect to $\Delta\boldsymbol{\theta}_i$ gives the Hessian,

$$\frac{\partial^2 \epsilon_i^*}{\partial \Delta\boldsymbol{\theta}_i{}^2} = 2 \left(\mathbf{S}_i^H \mathbf{W}_{\lambda_i} \mathbf{S}_i + \alpha^2 \mathbf{W}_{\theta_i} \right) \succ 0, \tag{37}$$

which is positive definite. Hence, ϵ_i^* is at least locally convex. This means that if convergence occurs, the solution is at least a local minimum of (15). To converge to the global minimum, it is important to have an initial guess $\boldsymbol{\theta}_0$, that lies sufficiently close to the global optimum. Hence, the original FE model should be a fairly good approximation of the real structure.

The above convergence proof will be valid in case only one set of the updating parameters $\boldsymbol{\theta}_p$ or $\boldsymbol{\theta}_z$ is used, while in the current IPZ model updating algorithm both are used. In this case, in order to come up with the updated structural stiffness matrix in each iteration, we need somehow to combine structure and substructure stiffness matrices based on step 2(j) of the algorithm. This calls for further investigation of the algorithm's convergence. According to (10) and (12), the new values of poles and zeros in each iteration are given by

$$[\boldsymbol{\lambda}_{n,p}]_{i+1} = [\boldsymbol{\lambda}_{n,p}]_i + \mathbf{S}_{pp} \Delta\boldsymbol{\theta}_p + \mathbf{S}_{pz} \Delta\boldsymbol{\theta}_z, \tag{38}$$

and

$$[\boldsymbol{\lambda}_{n,z}]_{i+1} = [\boldsymbol{\lambda}_{n,z}]_i + \mathbf{S}_{zp} \Delta\boldsymbol{\theta}_p + \mathbf{S}_{zz} \Delta\boldsymbol{\theta}_z. \tag{39}$$

However, after updating the structure and the substructure stiffness matrices, based on step 2(h) and 2(i), the substructure stiffness matrix will be replaced in the structure stiffness matrix according to step 2(j), thereby replacing a large part of the updated structure stiffness matrix. Although the cross-sensitivity terms smooth out the replacement step 2(j), this will result in a new set of poles $[\boldsymbol{\lambda}^{'}_{n,p}]_{i+1}$. In order to check whether step 2(j) compromises the convergence of the IPZ model updating algorithm as a whole, we can check if $\Delta\boldsymbol{\lambda}^{'}_{n,p} = [\boldsymbol{\lambda}^{'}_{n,p}]_{i+1} - [\boldsymbol{\lambda}_{n,p}]_i$ is still partly in the direction of

$$\Delta\boldsymbol{\lambda}_{n,p} = [\boldsymbol{\lambda}_{n,p}]_{i+1} - [\boldsymbol{\lambda}_{n,p}]_i = \mathbf{S}_{pp}\Delta\boldsymbol{\theta}_p + \mathbf{S}_{pz}\Delta\boldsymbol{\theta}_z. \tag{40}$$

This can be done by checking the following inner product

$$\gamma_{\lambda_p} := \frac{\Delta\boldsymbol{\lambda}_{n,p} \cdot \Delta\boldsymbol{\lambda}^{'}_{n,p}}{|\Delta\boldsymbol{\lambda}_{n,p}| \left|\Delta\boldsymbol{\lambda}^{'}_{n,p}\right|}. \tag{41}$$

In case $\gamma_{\lambda_p} > 0$, $\Delta\boldsymbol{\lambda}^{'}_{n,p}$ is partly in the direction of $\Delta\boldsymbol{\lambda}_{n,p}$, which means the replacement in step 2(j) partially preserves the updated poles of step 2(h). The usefulness of the convergence measure in (41) will be discussed with numerical results in the next section.

4. Simulation Results

In this section, a simulated pinned-sliding beam structure is used to illustrate the IPZ model updating method with combined sensitivities. In order to have a clean evaluation of the performance of the algorithm, we assumed a noise free environment. Noisy FRF data may result in less accurate estimations of the experimental poles and zeros and therefore in less accurate target values. This effect will be present in section 5 (to a minor extent), where real experimental FRFs will be used, but will obviously not play a role in the current section.

4.1. Case Study

Consider the 2D finite element model of a pinned-sliding aluminum beam with rectangular cross-section in Figure 1. The properties of the beam system are listed in Table 1. The beam is discretized by twelve Euler beam elements of equal size. Each element has two nodes and each node has two DOFs: a transversal displacement (w) and a rotation (r). The unreduced FE model has 24 DOFs in total. This model is referred to as the original model. It is assumed that the original model differs from the experimental structure in the sense that the 12^{th} element has a thickness of $3.0\ 10^{-2}\ m$ and a width of $1.333\ 10^{-2}\ m$ (instead of $2.0\ 10^{-2} m$ and $2.0\ 10^{-2} m$,

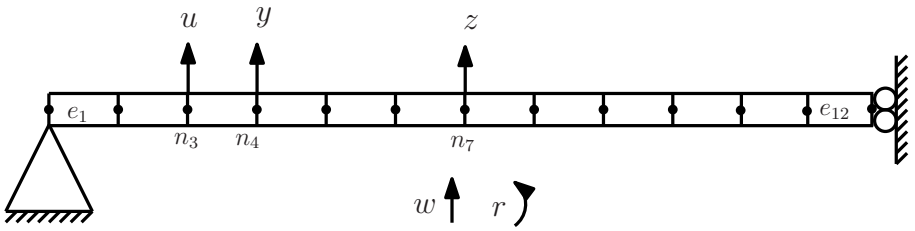

Figure 1: 2D aluminum beam system.

Table 1: Properties of the beam.

Property	Value	Unit
Young's modulus	69	GPa
Mass density	$2.7\ 10^{3}$	kgm^{-3}
Thickness	$2.0\ 10^{-2}$	m
Width	$2.0\ 10^{-2}$	m
Length	1.0	m

respectively). With this deviation, both the original and the experimental model still have the same cross sectional area and therefore the same mass, but a different second moment of area/inertia will result. Modal damping of 0.1% is added to all eigenmodes of both original and experimental model. Furthermore, assume that a force actuator (u) is located on the transversal displacement of the third node (n_3), a displacement sensor (y) is located on the transversal displacement of the fourth node (n_4), while the unmeasured performance variable (z) is assumed to be the transversal displacement of the seventh node (n_7). Now, the following FRFs can be introduced: $G_1 = Y/U$ and $G_2 = Z/U$, where the capital notation indicates the Fourier transform of the corresponding variables. By depicting the original numerical (G_n) and experimental (G_e) FRFs of G_1 and G_2 in Figure 2, a clear difference between pole and zero locations becomes visible.

In the context of unmeasured performance variables, displacement z is assumed to be located at the POI which means that G_2 cannot be measured directly. However, in this simulated experiment,

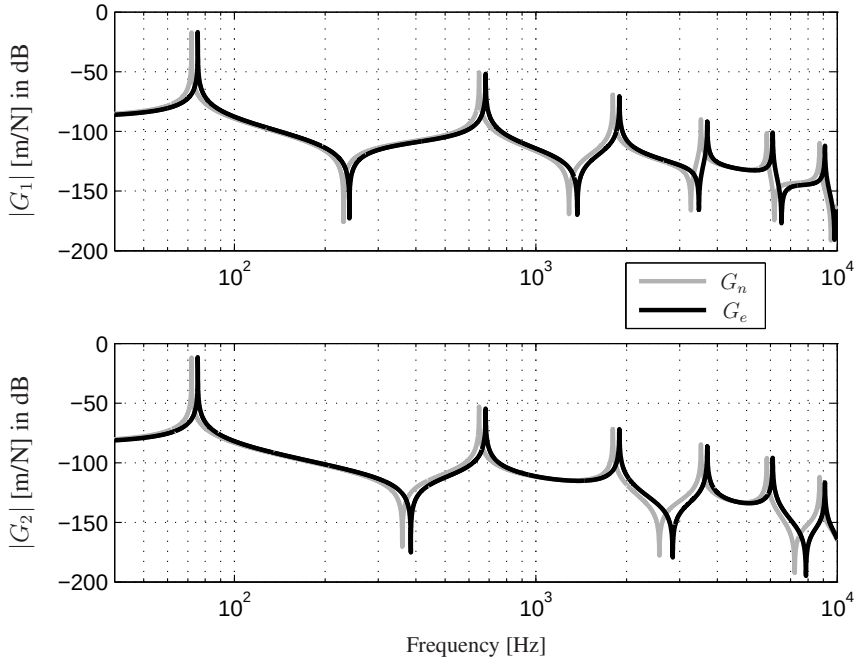

Figure 2: Original numerical (n) and experimental (e) $|G_1|$ (top) and $|G_2|$ (bottom).

the quality of the updated G_2 can be assessed since the "experimental" $G_{e,2}$ can be calculated from the "experimental" model. It will be assumed that in a real experiment the required experimental poles and zeros can be estimated from the measured FRFs by applying modal parameter fit procedures [19], [20]. Here, in the simulated experiment, they can simply be calculated. Note that poles and zeros resulting from (4) and (5) are assumed to occur in complex conjugated pairs since weak damping is assumed. In what follows, only the eigenvalues with positive imaginary parts will be used.

4.2. Simulation Results of IPZ Model Updating Using Combined Sensitivities

Now, model updating will be carried out. It is assumed that only G_1 is measured, therefore, the goal is to match the poles and zeros of the reduced-order G_1 with the poles and zeros of the experimental $G_{e,1}$ in the frequency range of interest, which is defined to be $[40, 5000]$ Hz. According to Figure 2, the first five flexible eigenmodes of the system are contributing most to this frequency range of interest. In addition, a residual flexibility mode is defined for the actuator DOF. Based on the selected number of modes and on the location of the actuator, sensor, and the POI, the following six transversal displacements $\mathbf{q}_r^T = [w_3, w_4, w_5, w_7, w_9, w_{11}]$ are selected as desired physical DOFs for model reduction. The original FRF $G_{n,1}$ and the reduced-order FRF $G_{r,1}$ are compared in terms of their amplitude in Figure 3. It can be seen that $G_{r,1}$ is a good approximation of $G_{n,1}$ within the frequency range of interest, which is shown by the black dashed-dotted lines.

Based on the frequency range of interest, the first four complex poles and the first three complex zeros of $G_{e,1}$ are assumed to be estimated. The first four complex poles of $G_{r,1}$ are chosen to be improved using the first four (real) eigenvalues of the reduced-order stiffness matrix $\mathbf{K}_r$ as generic updating parameters. The first three (complex-valued) zeros of $G_{r,1}$ are chosen to be improved using the second up to the fourth (real) eigenvalues of the substructure reduced-order stiffness matrix $\mathbf{K}_s$ because these eigenvalues show the highest sensitivity with respect to the selected zeros. Note that these generic updating parameters will mainly influence the imaginary parts of the poles and zeros. In case of non-collocated FRFs, the complete set of zeros includes real-valued zeros. It makes almost no sense to select design parameters which have large influence on the real-valued zeros. This is due to the fact that the real-valued poles/zeros are hardly identifiable from the measurement, and therefore cannot be included in the model updating process.

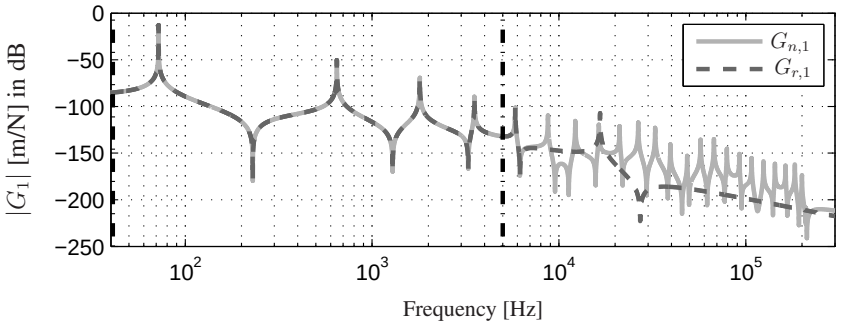

Figure 3: Original numerical $|G_{n,1}|$ and reduced-order $|G_{r,1}|$. The frequency range of interest is between the two vertical dashed dotted lines.

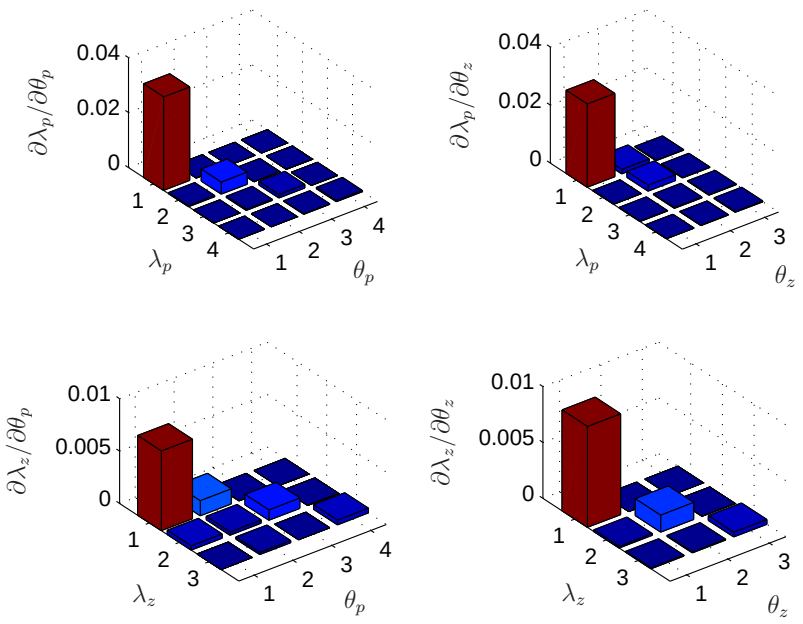

Figure 4: Sensitivity matrix ($\mathbf{S}_i$) in the first iteration. Derivatives of $[\lambda_{p,n,1}, \ldots, \lambda_{p,n,4}]$ w.r.t. $[\sigma_{p,1}, \ldots, \sigma_{p,4}]$ top left, $[\lambda_{z,n,1}, \ldots, \lambda_{z,n,3}]$ w.r.t. $[\sigma_{z,2}, \ldots, \sigma_{z,4}]$ bottom right, and the cross sensitivities in $G_{r,1}$.

In fact only the complex-valued poles and zeros with dominant imaginary parts can be estimated accurately. Here, the first eigenvalue of $\mathbf{K}_s$, is not selected as a zero updating parameter because it has large influence on the first zero which is real-valued. The sensitivities of the selected poles $[\lambda_{p,n,1}, \ldots, \lambda_{p,n,4}]$ w.r.t. the pole design parameters $[\sigma_{p,1}, \ldots, \sigma_{p,4}]$, the sensitivities of the selected zeros $[\lambda_{z,n,1}, \ldots, \lambda_{z,n,3}]$ w.r.t. the zero design parameters $[\sigma_{z,2}, \ldots, \sigma_{z,4}]$, and the cross-sensitivities are shown in Figure 4. It can be seen that the sensitivities of the poles w.r.t. the pole design parameters and the zeros w.r.t. the zero design parameters are diagonally dominant.

Using the IPZ model updating algorithm discussed in Section 3 with $\delta = 10^{-5}$, $\beta = 0.3$, and $\alpha = 0.1$, convergence is shown toward $\epsilon_i = 902.14$ in 20227 iterations. The choice for $\beta = 0.3$ is made because higher values of β do not lead to convergence. The number of iterations needed to converge toward a (local) minimum of (15) partially depends on the stop criterion parameter δ. Obviously, choosing a higher value for δ will generally result in a smaller number of iterations, but it also means that ϵ_i does not converge completely to its (local) minimum, i.e. the numerical poles and the zeros are not completely matched with the experimental values. For instance, using $\delta = 10^{-1}$ results in convergence to $\epsilon_i = 1108.6$ in 10019 iterations. Deviations of the updated poles and zeros with their corresponding experimental values using $\delta = 10^{-5}$ and $\delta = 10^{-1}$ are listed in Table 2. In general, deviations significantly decrease after model updating. Using $\delta = 10^{-5}$ in general results in lower deviations than using $\delta = 10^{-1}$, though the improvement is almost negligible. Although the number of iterations is relatively high, due to the fact that a reduced-order model is used and that the dimensions of the matrices are low, convergence can be

Table 2: Comparison of experimental (λ_e), numerical (λ_n), and updated (λ_u) poles (λ_p) and zeros (λ_z) for G_1.

	$\lambda_e\,(G_{e,1})$	$\lambda_n\,(G_{n,1})$	$\lvert(\lambda_n-\lambda_e)/\lambda_e\rvert\,\%$	$\lambda_u\,(G_{u,1})\;(\delta=10^{-5})$	$\lvert(\lambda_u-\lambda_e)/\lambda_e\rvert\,\%$	$\lambda_u\,(G_{u,1})\;(\delta=10^{-1})$	$\lvert(\lambda_u-\lambda_e)/\lambda_e\rvert\,\%$
λ_p	$-6.53\,10^{-3}+7.55\,10^{1}i$	$-5.46\,10^{-3}+7.20\,10^{1}i$	4.70	$-5.87\,10^{-3}+7.55\,10^{1}i$	$7.81\,10^{-3}$	$-5.85\,10^{-3}+7.56\,10^{1}i$	$9.26\,10^{-2}$
	$-3.26\,10^{-1}+6.81\,10^{2}i$	$-3.11\,10^{-1}+6.48\,10^{2}i$	4.87	$-2.80\,10^{-1}+6.81\,10^{2}i$	$7.71\,10^{-3}$	$-2.81\,10^{-1}+6.81\,10^{2}i$	$7.78\,10^{-3}$
	$-1.39\,10^{0}+1.89\,10^{3}i$	$-1.33\,10^{0}+1.80\,10^{3}i$	4.86	$-1.33\,10^{0}+1.89\,10^{3}i$	$3.55\,10^{-2}$	$-1.33\,10^{0}+1.89\,10^{3}i$	$1.66\,10^{-1}$
	$-2.99\,10^{0}+3.70\,10^{3}i$	$-2.88\,10^{0}+3.53\,10^{3}i$	4.70	$-2.90\,10^{0}+3.67\,10^{3}i$	$7.02\,10^{-1}$	$-2.90\,10^{0}+3.67\,10^{3}i$	$8.71\,10^{-1}$
λ_z	$-2.75\,10^{-2}+2.40\,10^{2}i$	$-2.48\,10^{-2}+2.29\,10^{2}i$	4.38	$-2.47\,10^{-2}+2.40\,10^{2}i$	$1.20\,10^{-3}$	$-2.47\,10^{-2}+2.40\,10^{2}i$	$7.63\,10^{-3}$
	$-8.68\,10^{-1}+1.37\,10^{3}i$	$-8.17\,10^{-1}+1.28\,10^{3}i$	6.11	$-8.13\,10^{-1}+1.37\,10^{3}i$	$1.11\,10^{-2}$	$-8.13\,10^{-1}+1.37\,10^{3}i$	$7.35\,10^{-3}$
	$-2.88\,10^{0}+3.47\,10^{3}i$	$-2.74\,10^{0}+3.26\,10^{3}i$	5.94	$-2.69\,10^{0}+3.49\,10^{3}i$	$4.08\,10^{-1}$	$-2.69\,10^{0}+3.48\,10^{3}i$	$1.13\,10^{-1}$

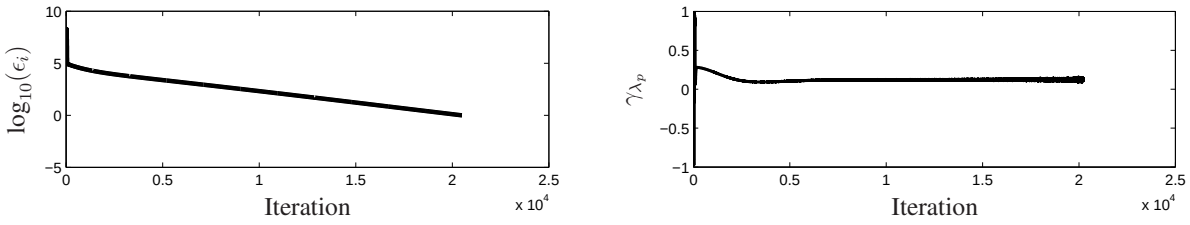

Figure 5: Convergence behavior of the IPZ model updating algorithm using G_1: (a) $\log_{10}(\epsilon_i)$ and (b) γ_{λ_p}.

accomplished within a few minutes using standard processing power.

Figure 5a shows that ϵ_i decreases rapidly during the first iterations and then decreases monotonically towards the (local) minimum until the stop criterion of (20) with $\delta = 10^{-5}$ is satisfied. Moreover, Figure 5b shows that $\gamma_{\lambda_p} > 0$ during the monotonic convergence phase (only in some initial iterations $\gamma_{\lambda_p} < 0$), which implies that the replacement in step 2(j) of the IPZ model updating algorithm partially preserves the initial direction of the updated poles in step 2(h). Convergence of the IPZ model updating toward a (local) minimum of (15) results in the updated reduced-order stiffness matrix $\mathbf{K}^u$, and thus in the updated reduced model composed of $\mathbf{M}_r$, $\mathbf{B}_r$, and $\mathbf{K}^u$. Figure 6 shows that $G_{u,1}$ (upper plot) matches very well in terms of both poles and zeros with the poles and the zeros of $G_{e,1}$ in the frequency range of interest. Moreover, the lower plot of Figure 6 shows that

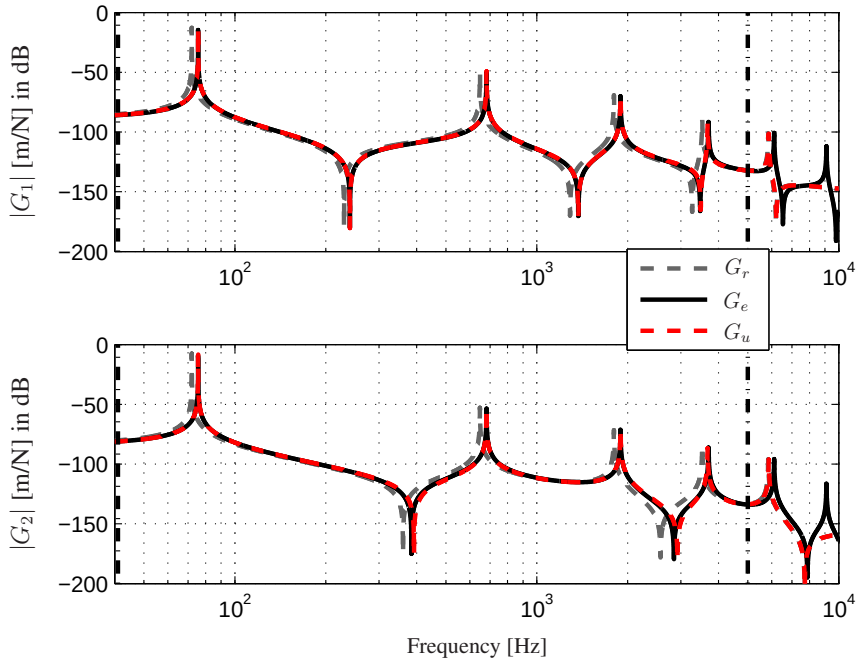

Figure 6: Original, experimental, and updated $|G_1|$ (top) and $|G_2|$ (bottom) after IPZ model updating. The frequency band of interest is indicated with black dotted-dashed lines.

Table 3: Correlation factors in the frequency range of interest before and after IPZ model updating using G_1

	$G_{r,1}$ vs. $G_{e,1}$	$G_{u,1}$ vs. $G_{e,1}$	$G_{r,2}$ vs. $G_{e,2}$	$G_{u,2}$ vs. $G_{e,2}$
X_S	0.025	0.946	0.026	0.336
X_A	0.004	0.950	0.004	0.954

$G_{u,2}$ also matches very well in terms of the poles and quite well in terms of the zeros with those from $G_{e,2}$. This is due to the well-known fact that the zero locations depend on the actuator/sensor location whereas the pole locations do not and are fixed. Both the shape (X_S) and amplitude (X_A) correlation measures of the FRFs [10], listed in Table 3, significantly improved after IPZ model updating. Note that the updated stiffness matrix has become non-symmetric whereas the original stiffness matrix is symmetric. A measure of non-symmetry which can be calculated via

$$\eta = \left|1/2(\mathbf{K}^u - \mathbf{K}^{uT})\right|_2 / \left|1/2(\mathbf{K}^u + \mathbf{K}^{uT})\right|_2, \tag{42}$$

is $3.38\,10^{-4}$ in this case, which is considered to be fairly small. Although an asymmetric stiffness matrix does not have physical interpretation in this example, it does not have any dynamic drawback either.

Experimental identification of compliance at the POI is not possible. The only solution is to calculate the compliance from the FE model, which may not be accurate enough. Updating the poles and the zeros through IPZ model updating not only improves the FRFs in the frequency range of interest, but also improves the compliance of the FRFs at the lower frequencies. Note that the residual flexibility mode incorporated in the model reduction step improves the compliance in the FRFs of the reduced-order model, but obviously it still may be different from the compliance in the measured FRFs. Figure 7 shows that the compliance of the updated G_2 is almost matched with the experimental compliance and that the compliance of the updated G_1 is clearly closer to the experimental values than the original model.

In case the cross-sensitivities are excluded from the model updating process, see (14), the algorithm converges to $\epsilon_i = 13.64$ in 920153 iterations. In this case, $\epsilon_i = 902.1$ occurs at iteration 432750. Thus, using cross sensitivities (in this case) speeds up the convergence rate with a factor of more than 21. The number of required iterations is still quite substantial for the case with cross-sensitivities. This is mainly caused by the replacement step 2(j) that largely undoes the pole updating step of 2(h) to quite some extent; see Figure 5b. If it does not hamper the convergence, also higher values of β speed up the convergence rate. For example, in the case without cross sensitivities, using $\beta = 1.9$ instead of $\beta = 0.3$, leads to convergence to $\epsilon_i = 8.12$ in 314199 iterations, thus about 3 times faster.

Note that the choice of desired DOFs $\mathbf{q}_r$ is an important step in model reduction since it may influence the convergence of IPZ model updating. Preferably, desired DOFs should be chosen such that modes of interest can be identified as linearly independent as possible, which basically means that $\boldsymbol{\phi}_s$ should be well-conditioned. In general, choosing very closely located DOFs will result in ill-conditioning of the IPZ model updating process. In this section, the number of DOFS of the original FE model is only 24, whereas in Section 2 it is mentioned that a typical model may contain 10^6 DOFs. Please note that the algorithm aims to update a reduced-order model within a

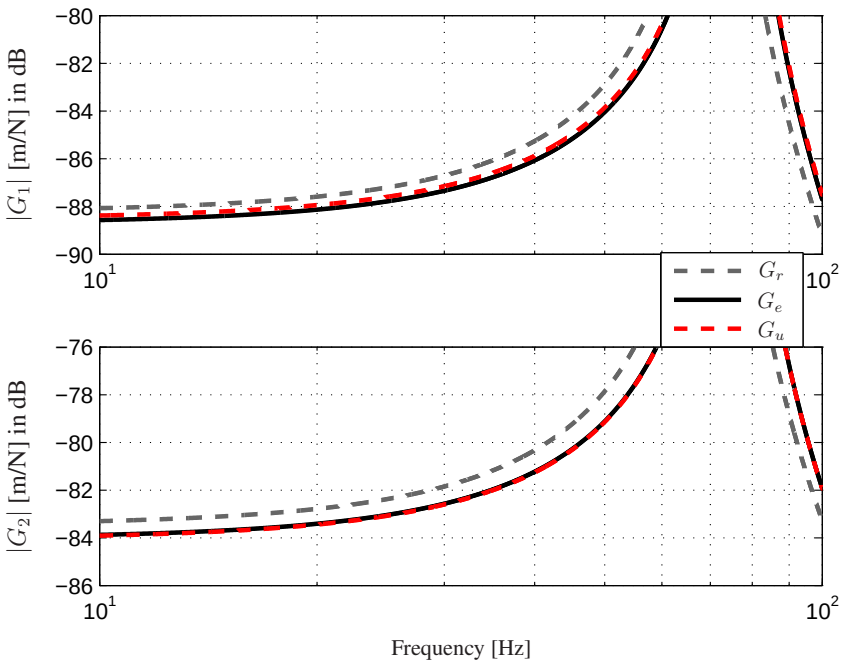

Figure 7: Reduced (r), experimental (e), and updated (u) $|G_1|$ (top) and $|G_2|$ (bottom).

frequency range of interest. Therefore, for the general application of the algorithm, the number of DOFs in the original FE model does not play a role, i.e. it may be high or low.

Recall that the algorithm is developed for situations where on beforehand, it is unknown where the main modeling errors are made. These unknown modeling errors may have a local nature (such as the local geometrical errors introduced in this example), but also may have a global nature (e.g. an error in the Youngs modulus). The algorithm aims at handling both situations (even the combination of both situations), because generic parameters (the eigenvalues of the stiffness and/or damping matrix) are used as updating parameters. Indeed, in the presented example, we do not use the knowledge that the error is in last element, and actually the locally introduced error is quite big. Still, the algorithm is capable of updating the model well using generic parameters.

Please note that in our line of application, where it comes to machine-to-machine variation, we may locally change the structure, while the original FE model is not updated accordingly. This may be due to the fact that updating the original large FE model on-site may be considered too expensive and too time consuming. Since from a control point of view we just need an accurate input-output model, IPZ model updating can provide such an updated reduced model fast. Although the locally introduced geometrical error in the example is not very realistic, since this data is often accurately known, this example does address to a certain extent the machine-to-machine variation problem.

5. Experimental Results

In this section, IPZ model updating is validated via non-collocated FRF measurement results from a cantilever beam setup. The experimental setup consists of a clamped-free aluminum beam as depicted in Figure 8. Two steel blocks are clamped together by four M10 bolts which are assumed to form an infinitely stiff clamping. The beam dimensions are chosen such that five eigenmodes are present in the frequency range of $[0, 1000]$ Hz. Geometrical and material properties of the beam are presented in Table 4. An accelerometer sensor (B&K, type: 8303, SN: 345018) is attached underneath point (a) in Figure 8 near the right end of the beam. The sampling frequency used in the experiments is $f_s = 2.56$ kHz. It is assumed that the POI indicated by (c) is located 24 cm from the clamp. Through modal hammer excitation at locations (b) and (c), two FRFs are measured, namely $G_{e,1}$ and $G_{e,2}$.

Note that in reality, for a cantilever beam, the main modeling error would probably be in the modeling of the clamping, and clamping stiffness properties would be the most obvious physical updating parameters. However, in this paper, we focus on the situation where we do not exactly know the source of the modeling error, as is often the case in geometrically complex structures. So, in this section, we will show that we still are able to successfully update the model using generic updating parameters without making use of the fact that the largest modeling error in this particular case is probably in the (infinitely stiff) modeling of the clamping.

The numerical FE model of the beam (G_n) is derived based on the properties listed in Table 4 and using 100 Timoshenko beam elements [26]. The FE model is built in MATLAB. Modal damping of 0.1% is assumed for all eigenmodes in the model. Then, a reduced model G_r is constructed using the first five flexible eigenmodes of the beam and a residual flexibility mode defined for location (a). The desired DOFs column is defined as $\mathbf{q}_r = [w_{15}, w_{55}, w_{95}(c), w_{135}, w_{175}(b), w_{199}(a)]^T$ corresponding to vertical displacements at respectively $[4, 14, 24, 34, 44, 49.95]$ cm from the clamp. It has been assumed that in a practical situation, only $G_{e,1}$ can be measured and that the vertical

Figure 8: Experimental clamped-free aluminum beam set up.

Table 4: Properties of the beam.

Property	Value	Unit
Young's modulus	69	GPa
Mass density	$2.69\ 10^3$	kgm^{-3}
Thickness	$5.1\ 10^{-3}$	m
Width	$25.33\ 10^{-3}$	m
Length	$499.5\ 10^{-3}$	m

displacement at location (c) is actually needed. Therefore, the goal is to update the reduced beam model based on $G_{e,1}$ such that the updated $G_{u,2}$ predicts $G_{e,2}$, i.e. dynamic behavior at location (c), more accurately than the original reduced model.

It is assumed that the frequency range of interest is $[10, 700]$ Hz. In this frequency range, the first four poles and the first three zeros of $G_{e,1}$ are estimated from the measurement. Therefore, the first four poles of $G_{r,1}$ are chosen to be updated using the first four (real) eigenvalues of the reduced-order stiffness matrix $\mathbf{K}_r$. Since $G_{e,1}$ is a non-collocated FRF, the first zero will be a real-valued zero which can not be identified easily from the measurement. Therefore, the first three complex-valued zeros of $G_{r,1}$ are chosen to be updated using the second up to the fourth (real) eigenvalues of the substructure reduced-order stiffness matrix $\mathbf{K}_s$. Figure 9a (top left and bottom right figures) shows that the selected poles and zeros have diagonal sensitivity w.r.t. the chosen pole and zero design parameters. The cross sensitivities between the poles and the zeros are shown in the top right and bottom left figures.

Using the stop criterion with $\delta = 10^{-3}$, ϵ_i practically converges toward a (local) minimum in about 590 iterations, see Figure 10a. If the cross sensitivities are not included in the IPZ model updating, it would take over 253000 iterations for ϵ_i to converge. As a result of updating the reduced stiffness matrix, $G_{u,1}$ matches reasonably well in terms of eigenfrequencies with the poles and the zeros of $G_{e,1}$, see the dashed blue curve in Figure 11a. However, after updating the stiffness, the updated model shows lower modal damping ratios than in the measured FRF. Therefore, the damping matrix is also updated to improve the modal damping ratios in the model. For updating the damping matrix, the chosen design parameters will be the first up to the fourth eigenvalues of the reduced-order damping matrix $\mathbf{B}_r$ along with the second up to the fourth eigenvalues of the substructure reduced-order damping matrix $\mathbf{B}_s$. The sensitivities of the previously selected poles and zeros w.r.t. the damping design parameters are shown in Figure 9b, where the top left and the

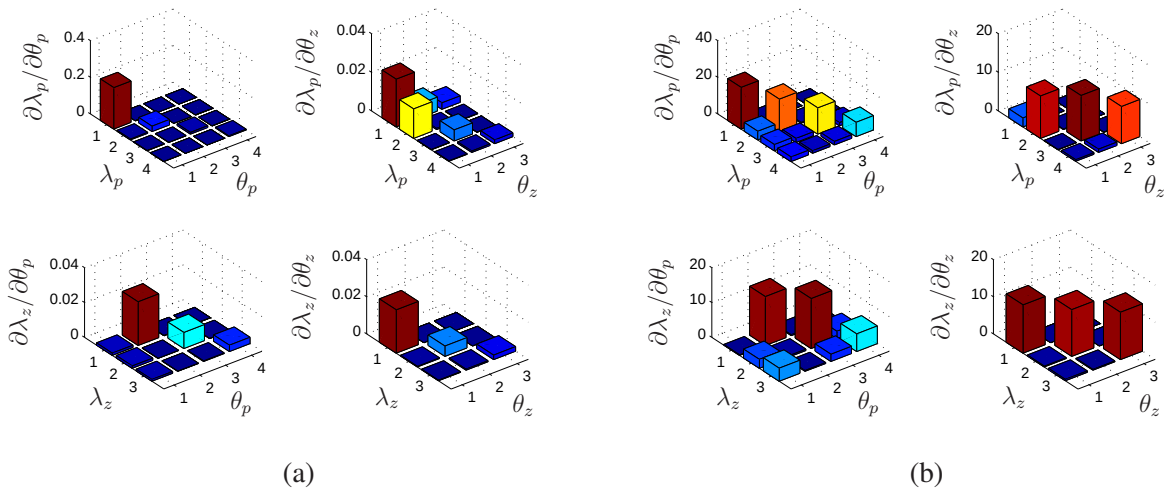

Figure 9: Sensitivity matrix ($\mathbf{S}_i$) in the first iteration for (a) stiffness updating and (b) damping updating. For both (a) and (b), sensitivities of $[\lambda_{p,n,1}, \ldots, \lambda_{p,n,4}]$ w.r.t. $[\sigma_{p,1}, \ldots, \sigma_{p,4}]$ on top left, sensitivities of $[\lambda_{z,n,1}, \ldots, \lambda_{z,n,3}]$ w.r.t. $[\sigma_{z,1}, \ldots, \sigma_{z,1}]$ on bottom right, and cross sensitivities on off diagonal plots.

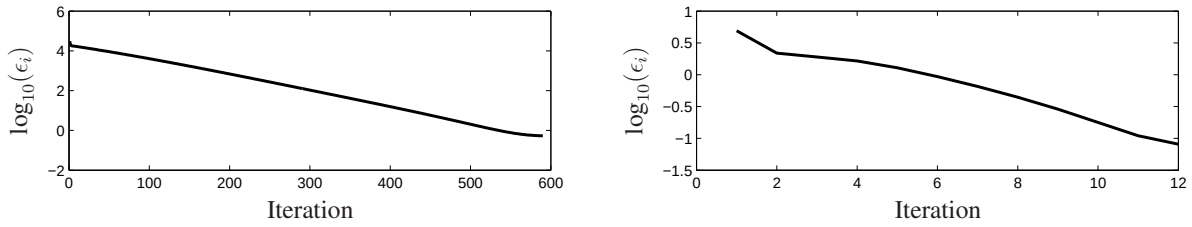

Figure 10: Convergence behavior of the IPZ model updating algorithm: $\log_{10}(\epsilon_i)$ for stiffness updating (a) and for damping updating (b).

bottom right figures show diagonally dominant sensitivities. When updating the damping matrix, ϵ_i practically converges toward a (local) minimum in just 12 iterations using the stop criterion with $\delta = 10^{-1}$. This has been shown in Figure 10b.

After updating the damping matrix, the poles and the zeros of $G_{u,1}$ match very well with the poles and the zeros of $G_{e,1}$, see the dashed red curve in Figure 11a. According to this figure, both amplitude and phase of the updated FRF matches with the experimental FRF. A comparison of original numerical, experimental and updated numerical values of the selected poles and zeros is presented in Table 5. The deviation of the poles and the zeros from the experimental values has been reduced significantly. Updating of the reduced stiffness matrix followed by updating of the reduced damping matrix also results in a much better match between the poles and the zeros of $G_{u,2}$ and $G_{e,2}$, see Figure 11b. It can be seen that the updated FRF at the POI in dashed-red matches very well in terms of both amplitude and phase with the experimental FRF in black. The shape (X_S) and amplitude (X_A) correlation measures, listed in Table 6, confirm significant improvement in correlation between the updated and the experimental FRFs of both G_1 and G_2 after updating the stiffness and damping based on G_1.

Table 5: Comparison of experimental (λ_e), numerical (λ_n), and updated (λ_u) poles (λ_p) and zeros (λ_z) for G_1.

	$\lambda_e\,(G_{e,1})$	$\lambda_n\,(G_{n,1})$	$\lvert(\lambda_n-\lambda_e)/\lambda_e\rvert\,\%$	$\lambda_u\,(G_{u,1})$	$\lvert(\lambda_u-\lambda_e)/\lambda_e\rvert\,\%$
λ_p	$-2.79\,10^{-1}+1.62\,10^{1}i$	$-1.09\,10^{-2}+1.66\,10^{1}i$	2.95	$-2.75\,10^{-1}+1.62\,10^{1}i$	$2.81\,10^{-2}$
	$-2.72\,10^{-1}+1.01\,10^{2}i$	$-6.89\,10^{-2}+1.04\,10^{2}i$	2.46	$-2.58\,10^{-1}+1.01\,10^{2}i$	$1.56\,10^{-2}$
	$-2.77\,10^{-1}+2.85\,10^{2}i$	$-1.93\,10^{-1}+2.92\,10^{2}i$	2.51	$-4.95\,10^{-1}+2.85\,10^{2}i$	$2.21\,10^{-1}$
	$-4.26\,10^{-1}+5.58\,10^{2}i$	$-3.78\,10^{-1}+5.73\,10^{2}i$	2.74	$-7.81\,10^{-1}+5.59\,10^{2}i$	$1.53\,10^{-1}$
λ_z	$-2.28\,10^{-1}+8.50\,10^{1}i$	$-5.12\,10^{-2}+8.73\,10^{1}i$	2.77	$-2.37\,10^{-1}+8.50\,10^{1}i$	$1.19\,10^{-2}$
	$-5.94\,10^{-1}+2.83\,10^{2}i$	$-1.91\,10^{-1}+2.90\,10^{2}i$	2.69	$-4.10\,10^{-1}+2.83\,10^{2}i$	$2.26\,10^{-1}$
	$-1.27\,10^{-1}+6.06\,10^{2}i$	$-4.26\,10^{-1}+6.22\,10^{2}i$	2.65	$-8.59\,10^{-1}+6.06\,10^{2}i$	$1.16\,10^{-1}$

Table 6: Correlation factors in the frequency range of interest before and after IPZ model updating using G_1

	$G_{r,1}$ vs. $G_{e,1}$	$G_{u,1}$ vs. $G_{e,1}$	$G_{r,2}$ vs. $G_{e,2}$	$G_{u,2}$ vs. $G_{e,2}$
X_S	0.194	0.926	0.141	0.839
X_A	0.220	0.980	0.216	0.959

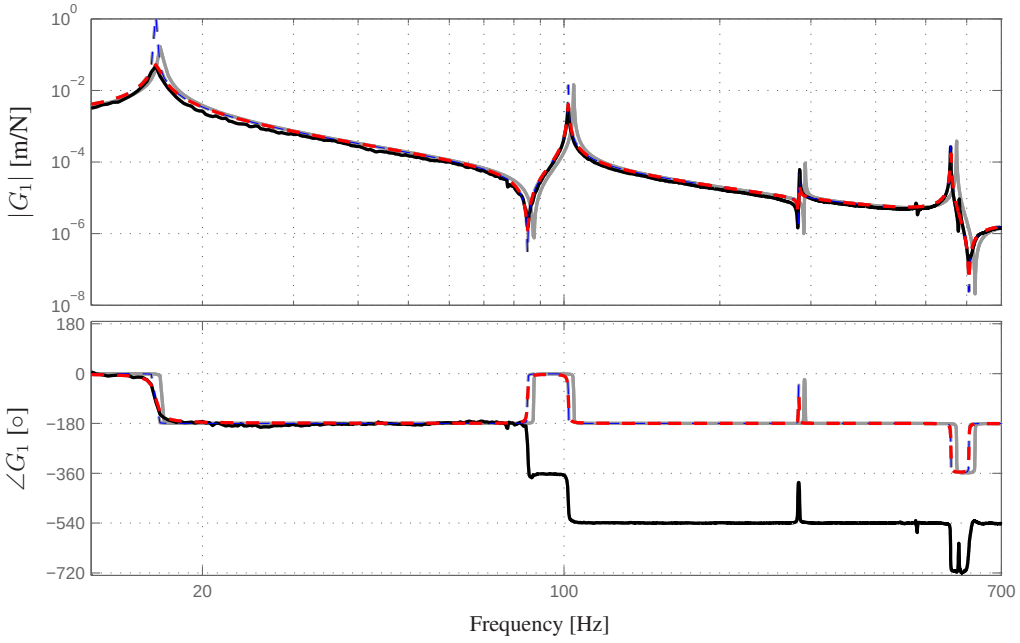

(a)

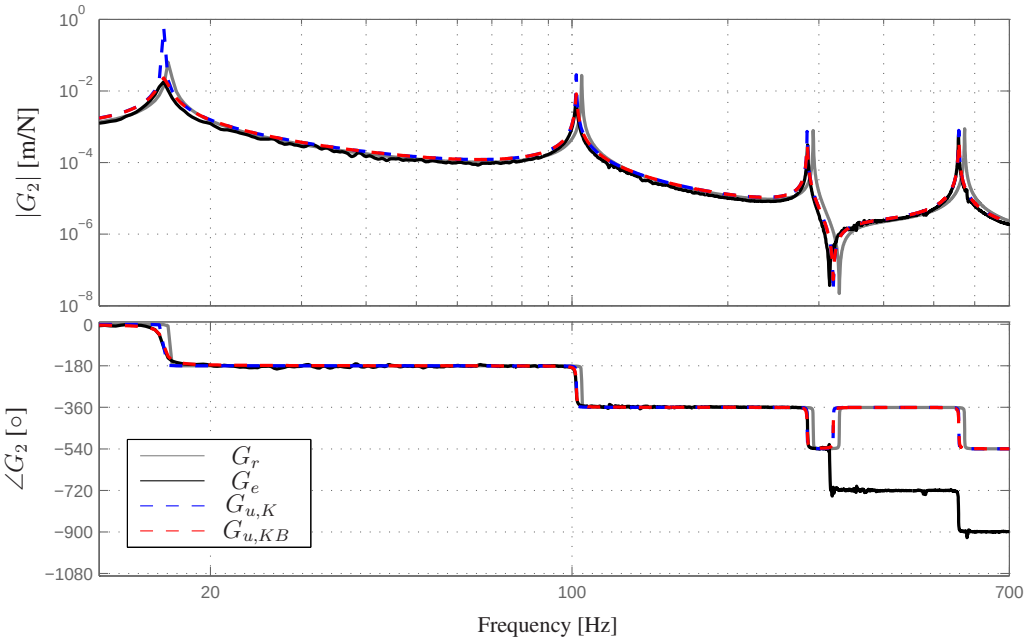

(b)

Figure 11: Experimental (G_e), reduced-order (G_r), stiffness updated ($G_{u,K}$), and (stiffness+damping) updated ($G_{u,KB}$) for G_1 (a) and G_2 (b).

6. Conclusions

In this paper, an IPZ model updating technique is introduced that uses combined sensitivities of the poles and the zeros with respect to generic updating parameters, and incorporates the cross sensitivities between the poles and zero updating parameters and vice versa. As updating generic parameters, the eigenvalues of the reduced (sub)structure stiffness/damping matrix are used. It should be remarked that for the model reduction step, the desired physical DOFs should be chosen carefully. It was shown that using these generic parameters we can improve the model accuracy. Through case studies with simulated and real experimental data it is demonstrated that incorporation of the cross sensitivities in the IPZ model updating will speed up the convergence rate significantly.

The still large number of iterations required for convergence is due to the sequence where the updated substructure stiffness matrix is replaced in the updated structure stiffness matrix, thereby canceling part of the information of the pole updating step. This is the price to be paid when desiring two matrices, i.e. the stiffness matrix and the substructure stiffness matrix to converge to one matrix in which the substructure stiffness matrix is part of the structure stiffness matrix. Note that in case of a non-collocated actuator/sensor configuration, the updated stiffness matrix will become non-symmetric, whereas the original stiffness matrix is symmetric. However, for the considered case studies the amount of non-symmetry remains fairly small and it seemingly does not have any dynamic drawback in the updated model.

IPZ model updating using combined sensitivities has been validated using non-collocated FRF measurement results from a cantilever beam setup. The experimental results show that the updated numerical model not only match very well with the measured FRF, but it can also predict quite well the immeasurable FRF at the POI. Note that IPZ model updating with combined sensitivities can be applied on both collocated as well as non-collocated FRFs. In summary, IPZ model updating pose a solution to the problem of obtaining accurate predictions of unmeasured performance variables at the POI that cannot be readily measured.

The focus of this paper is on lightly damped structures with application in wafer scanners, electron microscopes, aerospace structures, and medical systems. A recommendation for future research is to investigate if the IPZ model updating method can be successfully applied to more heavily damped structures, for which it will be more challenging to accurately estimate the experimental poles and zeros. Once these quantities are obtained, in principle the presented IPZ model updating method can be applied, but full understanding of the implications of higher damping levels will require more research.

The cantilever beam system considered in Section 5 is still a simple structure, but this case study already contains quite some very relevant aspects for model updating: there is modeling uncertainty due to the clamping and unknown damping, model reduction is applied, noise is present in the experimental data, and fitting procedures are used to estimate the experimental poles and zeros. The authors are planning to validate the method on more complex structures in a future paper. Additional aspects which will be considered there will be closely spaced poles and closely spaced zeros.

References

[1] M. van de Wal, G. van Baars, F. Sperling, O. Bosgra, Multivariable H_∞/μ feedback control design for high-precision wafer stage motion, Control Engineering Practice 10 (2002) 739–755.

[2] M. G. Wassink, M. van de Wal, C. Scherer, O. Bosgra, LPV control for a wafer stage: beyond the theoretical solution, Control Engineering Practice 13 (2005) 231–245.

[3] S. Devasia, E. Eleftheriou, S. O. R. Moheimani, A survey of control issues in nanopositioning, IEEE Transactions On Control Systems Technology 15 (5) (2007) 802–823.

[4] V. Arora, Comparative study of finite element model updating methods, Journal of Vibration and Control 17 (13) (2011) 2023–2039.

[5] J. E. Mottershead, M. Link, M. I. Friswell, The sensitivity method in finite element model updating: A tutorial, Mechanical Systems and Signal Processing 25 (2011) 2275–2296.

[6] B. Jaishi, W.-X. Ren, Finite element model updating based on eigenvalue and strain energy residuals using multiobjective optimisation technique, Mechanical Systems and Signal Processing 21 (2007) 2295–2317.

[7] M. Dorosti, R. Fey, M. Heertjes, M. van de Wal, H. Nijmeijer, Finite element model reduction and model updating of structures for control, in: 19th World Congress, The International Federation of Automatic Control (IFAC), Cape Town, South Africa, 2014.

[8] V. Arora, S. Adhikari, M. Friswell, FRF-based finite element model updating method for non-viscous and non-proportional damped system, in: International conference on structural engineering dynamics, Lagos, Portugal, 2015.

[9] T. Abrahamsson, F. Bartholdsson, M. Hallqvist, K. Olsson, M. Olsson, A. Sallstrom, Calibration and cross-validation of a car component using frequency response functions and a damping equalization technique, in: Proceedings of ISMA2014 including USD2014, Leuven, Belgium, 2014.

[10] M. Dorosti, F. Heck, R. Fey, M. Heertjes, M. van de Wal, H. Nijmeijer, Frequency response sensitivity model updating using generic parameters, in: American Control Conference (ACC), Boston, 2016.

[11] B. Jaishi, W.-X. Ren, Structural finite element model updating using ambient vibration test results, Journal of Structural Engineering 131 (2005) 617–628.

[12] B. Titurus, M. I. Friswell, L. Starek, Damage detection using generic elements: Part i. model updating, Computers and Structures 81 (2003) 2273–2286.

[13] H. Ahmadian, G. M. L. Gladwell, F. Ismail, Parameter selection strategies in finite element model updating, Journal of Vibration and Acoustics 119 (1997) 37–45.

[14] V. Arora, Constrained antiresonance frequencies based model updating method for better matching of FRFs, Inverse Problems in Science and Engineering 22 (6) (2014) 873–888.

[15] W. D'Ambrogio, A. Fregolent, Results obtained by minimising natural frequency and antiresonance errors of a beam model, Mechanical Systems and Signal Processing 17 (1) (2003) 29–37.

[16] D. Hanson, T. Waters, D. Thompson, R. Randall, R. Ford, The role of anti-resonance frequencies from operational modal analysis in finite element model updating, Mechanical Systems and Signal Processing 21 (2007) 74–97.

[17] K. Jones, J. Turcotte, Finite element model updating using antiresonant frequencies, Journal of Sound and Vibration 252 (4) (2002) 717–727.

[18] J. E. Mottershead, On the zeros of structural frequency response functions and their sensitivities, Mechanical Systems and Signal Processing 12 (5) (1998) 591–597.

[19] A. Phillips, R. Allemang, D. Brown, Autonomous modal parameter estimation: Methodology, Conference Proceedings of the Society for Experimental Mechanics Series 6 Modal Analysis Topics, Volume 3 (2011) 363–384.

[20] M. El-Kafafy, P. Guillaume, B. Peeters, Modal parameter estimation by combining stochastic and deterministic frequency-domain approaches, Mechanical Systems and Signal Processing 35 (2013) 52–68.

[21] H. Ahmadian, J. E. Mottershead, M. I. Friswell, Regularisation methods for finite element model updating, Mechanical Systems and Signal Processing 12 (1) (1998) 47–64.

[22] B. Titurus, M. I. Friswell, Regularization in model updating, International Journal For Numerical Methods In Engineering 75 (2008) 440–478.

[23] M. I. Friswell, J. E. Mottershead, H. Ahmadian, Finite-element model updating using experimental test data:

parametrization and regularization, Philosophical Transactions of the Royal Society of London: Mathematical, Physical and Engineering Sciences 359 (2001) 169–186.
[24] J. Silva, N. Maia, Modal Analysis and Testing, Kluwer Academic Publication, 1999, Ch. Updating of Analytical Models - Basic Procedures and Extensions, pp. 281–304.
[25] T. J. Ypma, Historical development of the newton-raphson method, Society for Industrial and Applied Mathematics (SIAM) 37 (4) (1995) 531–551.
[26] R. Davis, R. D. Henshell, G. B. Warburton, A Timoshenko beam element, Journal of Sound and Vibration 22 (4) (1972) 475–487.